BCSJ Award Article

Complex Formation between a Nucleobase and Tetracyanoquinodimethane Derivatives: Crystal Structures and Transport Properties of Charge-Transfer Solids of Cytosine[1]

Tsuyoshi Murata,*[1] Gunzi Saito,*[1,2] Kazukuni Nishimura,[1] Yuichiro Enomoto,[1] Genki Honda,[1] Yasuhito Shimizu,[1] Shogo Matsui,[1] Masafumi Sakata,[1] Olga O. Drozdova,[3] and Kyuya Yakushi[3]

[1]Division of Chemistry, Graduate School of Science, Kyoto University, Sakyo-ku, Kyoto 606-8502

[2]Research Center for Low Temperature and Materials Sciences, Kyoto University, Sakyo-ku, Kyoto 606-8502

[3]Institute for Molecular Science, Okazaki 444-8585

Received August 8, 2007; E-mail: saito@kuchem.kyoto-u.ac.jp

Reaction between cytosine, a nucleobase, in methanol and several 7,7,8,8-tetracyanoquinodimethane derivatives (R-TCNQ) in acetonitrile yielded three kinds of ionic solids; (**I**) insulators composed of methoxy-substituted R-TCNQ anions, (**II**) semiconducting fully ionic R-TCNQ radical anion salts, and (**III**) conductive partially ionic or mixed-valent R-TCNQ radical anion salts. Electronic and chemical structures of these products were characterized by optical and magnetic measurements, and structural and elemental analyses. Cation units in all products were found to be protonated cytosine species. Crystal structures were determined for methoxy-substituted anion salts (R = F_4 and H) in Group **I** and R-TCNQ radical anion salts (R = H and Et_2) in Group **II** with hemiprotonated cytosine pairs formed by triple self-complementary hydrogen bonds. They established one-dimensional hemiprotonated cytosine ribbons by double complementary hydrogen bonds. Hydrogen bonds between cytosine and R-TCNQ anions exhibited high potential to regulate molecular arrangements producing a segregated layered structure and uniform arrangement of R-TCNQ radical anion columns stable down to low temperature. The partially ionic salt of MeTCNQ in Group **III** exhibited metallic behavior and the highest conductivity of 10^{+1} S cm^{-1} so far observed for charge-transfer complexes based on biological molecules.

Biological molecules such as proteins, enzymes, DNA, etc., establish well-defined and complicated self-assembling structures which are important factors in the exhibition of their biological functions. This feature of biological molecules has attracted much attention from the viewpoint of supramolecular chemistry and crystal engineering in recent study of molecule-based materials.[2] In research for organic conductors, several attempts to investigate charge-transfer (CT) complexes based on a variety of biological molecules have been also undertaken.[3]

Hydrogen-bond (HB) interaction has been recognized as one of the most important interactions in the formation of biological molecular architectures.[2a,4] For example, the selective base-pair formation of nucleobases by complementary HBs connects two oligonucleotides to form double-stranded DNA molecules.[5] This feature of nucleobases has been utilized in the construction of self-assembled structures.[2a,4,6] To control the molecular arrangement in organic conductors, several conductive CT solids with nucleobase skeletons have been developed in TTF (tetrathiafulvalene) systems having uracil moieties ($\sigma_{RT} = 10^{-1}$–2 S cm^{-1}, RT = room temperature)[7] and betainic radicals of pyrimido-fused-TTF derivatives ($\sigma_{RT} = 10^{-1}$ S cm^{-1} at most).[8] For some of these TTF derivatives, the construction of well-defined assembled structures based on complementary HBs has been also disclosed by structural analyses.

CT complexes composed of nucleobases themselves have also been investigated, although highly conductive ones have not been realized.[9–11] In the complex formation of nucleobases with *p*-chloranil, only guanine (**G**) gave a CT solid which was assumed to be in the neutral ground state from the optical spectrum.[9] Although there were no conductivity data, the electronic structure suggested that this solid was an insulator. Bazhina et al. studied the CT solids of TCNQ (7,7,8,8-tetracyanoquinodimethane, Chart 1) with **G**; however, no conductivity data was provided, and only the mobility of electrons was described with regard to the transport properties of the salt.[10] Later, Sheina et al. examined the reaction between nucleobase derivatives in methanol (MeOH) and TCNQ in acetonitrile (MeCN) and investigated the stoichiometry of the resulting solid products and ionicity of TCNQ molecules based on spectroscopic studies in solution.[11] Among them, cytosine (**C**, Chart 1) and 1-methylcytosine gave dark blue TCNQ radical anion salts with 2:1 stoichiometry; however, no information about the

Published on the web March 13, 2008; doi:10.1246/bcsj.81.331

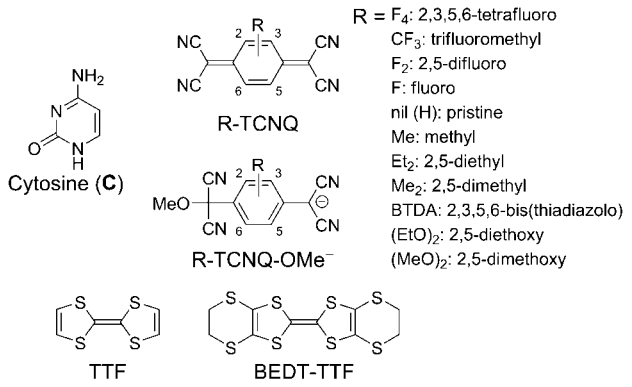

Chart 1. Chemical structures of compounds in text.

electronic structure of **C** was given. The stoichiometry suggested four possible **C** species: $(\mathbf{C}^0\mathbf{C}^{\bullet+})$, $(\mathbf{C}^{0.5\bullet+})_2$, $(\mathbf{C}^0\mathbf{CH}^+)$, and $(\mathbf{C_2H}^+)$. The former two species contain radical cation, and the latter two are protonated **C** species. Conductivity and structural analyses of these solid products were not studied.

Estimation of ionization potentials (I_p) shows that they should be effective π-donors, particularly in the case of **G**; $I_p = 7.64$–7.85 eV vs. adenine (7.80–8.26 eV), cytosine **C** (8.45–8.74 eV), and thymine (8.74–8.87 eV).[12] However, compared with TTF ($I_p = 6.4$ eV,[13a] oxidation potential ($E_{1/2}{}^{ox}$) = +0.35 V vs. SCE in MeCN), **C** ($E_p{}^{ox} = +1.90$ V vs. SCE in MeCN)[14] is too poor an electron donor to ionize conventional acceptor molecules. TCNQ (reduction potential ($E_{1/2}{}^{red}$) = +0.22 V vs. SCE in MeCN) gives neutral and partially ionic CT complexes with BEDT-TTF ($I_p = 6.21$ eV,[13b] $E_{1/2}{}^{ox}$ = +0.53 V vs. SCE in MeCN), whose electron-donating ability lies on the boundary for ionization of TCNQ. To create radical salts between **C** and TCNQ, where significant CT is impossible as far as only their redox properties are concerned, the lattice energy must be increased by 2.24 eV from I_p or 1.37 eV from redox potentials. In addition, the radical cation $\mathbf{C}^{\bullet+}$ is known to be very unstable because of rapid deprotonation of the highly acidic N–H group to generate neutral radical species.[15] Considering these features of **C**, generation of $\mathbf{C}^{\bullet+}$ species in a **C**–TCNQ CT solid reported by Sheina et al.[11] is hardly expected, and protonated **C** species are more preferable as the cation part.

Examination of CT solids with a series of acceptor molecules having a wide range of electron affinity and a constant size and shape is essential for the development of new conducting systems and for the elucidation of roles of a specific nucleobase in transport properties.[16] To explore biological molecule based conductors having self-assembled structures and to clarify the generation mechanism of TCNQ radical anion species in the reaction with **C** reported by Sheina et al.,[11] we have studied CT complex formation between **C** and a series of TCNQ derivatives (R-TCNQ, Chart 1). Here, we report the reaction between **C** and R-TCNQ in the presence of MeOH as solvent, characterization of the products based on elemental, optical, and structural analyses, electronic properties by transport and magnetic measurements, and the self-assembled structures formed by the complementary HB interactions of **C** molecules in their crystal structures. We emphasize that (1) despite the weak electron-donating ability of **C**, the reaction produced radical anion salts of R-TCNQ with protonated **C** cations, where alcoholysis of R-TCNQ and strong proton-affinity of **C** are the key factors in the reaction mechanism, (2) the robust HB interaction and π-stacking inherent in **C** controlled the crystal and electronic structures of the R-TCNQ assemblies, and (3) our investigation demonstrated the first metallic CT solid constructed from nucleobases themselves.

Results and Discussion

Preparation and Classification of Products. Table 1

Table 1. Appearance and Optical Properties of the Reaction Products between **C** and R-TCNQ

R ($E_{1/2}{}^{red}$ a))	No.	Solid color, shape	IR $\nu_{C\equiv N}$ f)/cm^{-1}			UV–vis–NIR g)/10^3 cm^{-1}						
			A^0	$A^{\bullet-}$	Product	A	B	C	D	E	E′	F
F_4 (+0.60)	**1** b)	Pale yellow, needles	2227	2212	2193, 2153 [40]						29.2	36.2
	2 b)	Blue, needles			2200, 2181		7.9	9.9, 11.5	14.9	26.7		37.0
CF_3 (+0.44)	**3**	Pale green, d) powder	2223	2201	2183, 2134 [49]						30.3	36.2
F_2 (+0.41)	**4**	Pale green, d) powder	2230	2201	2182, 2130 [52]						28.9	36.5
	5	Blue-purple, needles			2197, 2172		6.8	11.7	16.2	26.3		37.0
F (+0.32)	**6**	Pale yellow, powder	2221	2201	2181, 2132 [49]						29.4	36.8
	7	Blue-purple, needles			2192, 2176, 2163		7.2	11.6	16.3	27.3		37.0
H (+0.22)	**8** e)	Pale green, d) powder Pale yellow, plates	2222	2196	2178, 2124 [54]						29.8	36.5
	9 c)	Black, plates			2187, 2170, 2157		7.1	11.8	16.4	27.6		37.3
	10	Black, microcrystals			2188, 2170, 2157		7.0	11.7	16.4	27.9		37.3
Me (+0.19)	**11**	Green, d) powder	2223	2190	2178, 2133 [55]						29.9	37.3
	12	Black, needles			2202, 2082	3.4		10.4, 11.5	17.5	26.2		37.9
Et_2 (+0.15)	**13**	Green, plates	2213	2184	2183, 2150		7.5	12.0	14.2	25.5		36.2
Me_2 (+0.15)	**14**	Dark blue, powder	2222	2183	2184, 2172, 2158	3.4	6.2	11.8	16.7	26.5		37.0

a) Reduction potentials of R-TCNQ in V vs. SCE in MeCN. b) See Ref. 1a. c) See Ref. 1b. d) Green color of **3**, **4**, **8** (powder), and **11** is ascribed to the minute contamination of radical anions by the corresponding R-TCNQ. e) The powder and crystal samples of **8** contain water or MeOH as crystal solvents, respectively. f) A^0: neutral R-TCNQ and $A^{\bullet-}$: R-TCNQ radical anion. Numbers in square brackets are frequency differences ($\Delta\nu_{C\equiv N}$). g) Bands A–F: see text. The prime of Band E′ means that the band originates from R-TCNQ-OMe$^-$ species.

Table 2. Assignment and Electrical Conductivity of the Products

R	No.	Group	Assignment and composition	σ_{RT}/S cm^{-1} (ε_a/eV)
F_4	**1**[a]	**I**	(**CHC**$^+$)(F_4TCNQ-OMe$^-$)(H_2O)[c]	Insulator[g]
	2[a]	**II**	(**CHC**$^+$)(F_4TCNQ$^{\bullet-}$)[d]	5.3–6.4 × 10^{-9} (0.43–0.45)[g]
CF_3	**3**	**I**	(**CHC**$^+$)(CF_3TCNQ-OMe$^-$)(H_2O)$_{0.5}$[d]	Insulator[g]
F_2	**4**	**I**	(**C$_3$H**$^+$)(F_2TCNQ-OMe$^-$)(H_2O)$_{0.5}$[d]	Insulator[g]
	5	**II**	(**CHC**$^+$)(F_2TCNQ$^{\bullet-}$)[d]	1.0–1.4 × 10^{-3} (0.21)[g]
F	**6**	**I**	(**CHC**$^+$)(FTCNQ-OMe$^-$)(H_2O)[d]	Insulator[g]
	7	**II**	(**CHC**$^+$)(FTCNQ$^{\bullet-}$)[d]	5.8 × 10^{-4} (0.17)[g]
H	**8**	**I**	(**CHC**$^+$)(TCNQ-OMe$^-$)(H_2O)$_{0.9}$ (powder)[d]	Insulator[g]
			(**CHC**$^+$)(TCNQ-OMe$^-$)(MeOH) (crystal)[c,e]	
	9[b]	**II**	(**CHC**$^+$)(TCNQ$^{\bullet-}$)[c,d]	2.7–3.2 × 10^{-2} (0.14)[h]
	10	**II**	(**CH**$^+$)(TCNQ$^{\bullet-}$)(H_2O)$_{0.5}$[d]	1.1 × 10^{-4} (0.12)[g]
Me	**11**	**I**	(**CHC**$^+$)(MeTCNQ-OMe$^-$)(H_2O)$_{0.3}$(MeCN)[d]	Insulator[g]
	12	**III**	(**CHC**$^+$)(MeTCNQ$^{0.5\bullet-}$)$_2$[d]	2.7–7.2 × 10^{+1} (metallic, $T_{\sigma max}$ = 273–289 K)[h]
Et_2	**13**	**II**	(**CHC**$^+$)(Et_2TCNQ$^{\bullet-}$)[c,d]	0.4–1.3 × 10^{-4} (0.18–0.19)[g]
Me_2	**14**	**III**	(**C$_3$H**$^+$)$_2$(Me_2TCNQ$^{2/3\bullet-}$)$_3$(H_2O)[d,f]	2.6–4.7 × 10^{-2} (0.081–0.085)[g]

a) See Ref. 1a. b) See Ref. 1b. c) Composition was estimated by X-ray crystal structure analysis. d) Composition was estimated by elemental analysis. e) Recrystallization from MeOH afforded the salt **8** including the solvent molecule. f) **14** has non-uniform charge, and the charge on the Me_2TCNQ moiety is an averaged one. g) Measured on compressed pellet samples. h) Measured on single crystals.

summarizes the color, shape, and spectral characteristics of the solid products **1**–**14**, according to the acceptor strengths. Reactions were performed by mixing the solutions of **C** in dry MeOH, which is the best organic solvent to dissolve **C**, and R-TCNQ in dry MeCN at RT in molar ratios from 2:1 to 1:2. No difference was found when mixed under open air or anhydrous conditions (dry solvents under inert gas). Mixing a yellow-orange solution of R-TCNQ and a colorless one of **C** afforded blue-green solutions, of which optical spectra showed characteristic absorption bands of R-TCNQ$^{\bullet-}$ species. The speed of coloration and the following precipitation of solids depended on the acceptor species. The mixed solutions with strong acceptors (R = F_4, CF_3, F_2, and F) turned to blue-green immediately, and in many cases no CT solid appeared until the mixed solutions became almost dry or were cooled down to −18 °C, indicating that the products had high solubility in MeOH/MeCN. In the cases of weak R-TCNQ (R = H, Me, and Et_2), the green color appeared gradually, and the dark-colored CT solid precipitated within 1 day. Slow diffusion of **C** and TCNQ in MeOH/MeCN (2:1) solution afforded single crystals of **9**. **9** was also prepared by metathesis reaction using ternary species; equimolar portions of **C**, **C** hydrochloride (**CH**$^+$·Cl$^-$), and Li$^+$·TCNQ$^{\bullet-}$. In the complex formation with Me_2TCNQ, the color changed very slowly (2 weeks), and solid **14** precipitated from the concentrated reaction mixture. In the case of BTDA-TCNQ ($E_{1/2}^{red}$ = +0.03 V vs. SCE in MeCN), the green color of the reaction mixture immediately faded probably due to decomposition of radical anion species of the acceptor. In the mixing with very weak acceptors ((MeO)$_2$TCNQ; $E_{1/2}^{red}$ = +0.05 V and (EtO)$_2$TCNQ; $E_{1/2}^{red}$ = +0.01 V vs. SCE in MeCN), color change showing the R-TCNQ$^{\bullet-}$ species was not observed.

The C≡N stretching modes in the IR spectra indicated that the R-TCNQ species in the solids were not neutral species. IR and UV–vis–NIR spectra classified the products into three groups: (**I**) ionic salts with destructed R-TCNQ anions, which were characterized as methoxy-substituted R-TCNQ anions (R-TCNQ-OMe$^-$, Chart 1); (**II**) fully ionic CT salts of R-TCNQ$^{\bullet-}$; and (**III**) partially ionic (uniform charge) and mixed-valent (non-uniform charge) CT salts of R-TCNQ$^{\delta\bullet-}$ ($0 < \delta < 1$). Table 2 summarizes the assignment of the solid products together with their transport properties. The elemental analyses of the purified substances were consistent with calculated ones within experimental error limits (0.3% for each element, see Supporting Information).

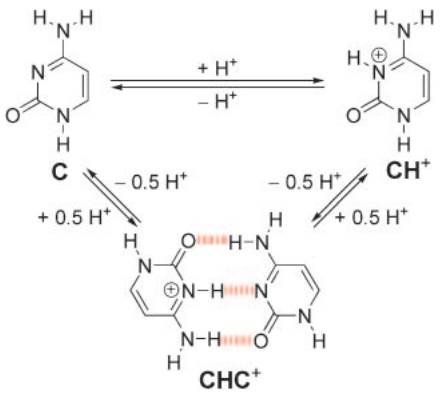

Scheme 1. Protonation process of **C** species.

Reaction Mechanism. **C** is a Brønsted acid as well as a base (pK_a = 4.55 and 12.2)[17] that readily forms a protonated cation (**CH**$^+$) in acidic conditions. In addition to **C** and **CH**$^+$ species, half-protonation gives a pair of **C** and **CH**$^+$, namely a hemiprotonated **C** pair (**CHC**$^+$) formed by the triple complementary HBs (Scheme 1). **CHC**$^+$ species have rarely been observed in several salts of **C** derivatives.[7f,18] IR spectra and structural analyses of the reaction products between **C** and R-TCNQ indicated that their cation parts were protonated cytosine species (vide infra). On the other hand, according to structural analyses of **1**[1a] and **8** (vide infra), the destructed R-TCNQ products were characterized as methoxy adduct anions, R-TCNQ-OMe$^-$, and the salts were formulated as (**CHC**$^+$)(R-TCNQ-OMe$^-$). The optical, ^{1}H NMR, and elemental analyses

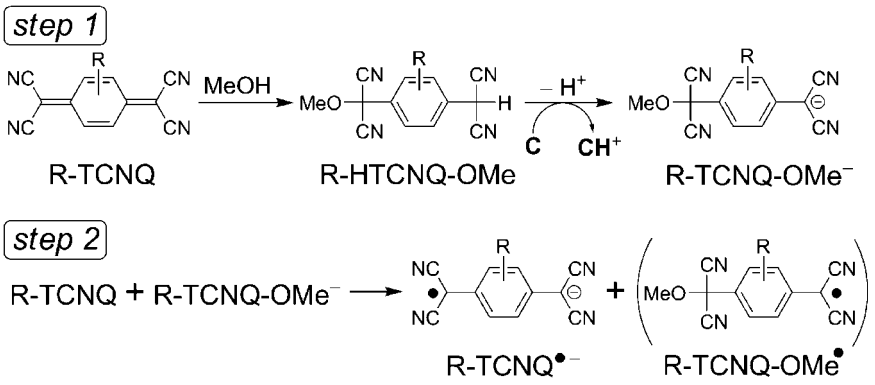

Scheme 2. Formation mechanism of the reaction products, R-TCNQ-OMe$^-$ and R-TCNQ$^{\bullet-}$.[1a,19]

of other salts in Group **I** (**3**, **6**, and **11**, Tables 1 and 2) indicated that they had the same formula to those of **1** and **8**. Only **4** was characterized as ($\mathbf{C_3H}^+$)(F_2TCNQ-OMe$^-$), where $\mathbf{C_3H}^+$ is an unknown species. R-TCNQ-OMe$^-$ species in these salts were produced by the methanolysis reaction of R-TCNQ acceptors and the deprotonation by **C** (Scheme 2, step 1).[1a,19,20]

Cyclic voltammetry measurements of R-TCNQ-OMe$^-$ salts (see Supporting Information), where R-TCNQ-OMe$^-$ exhibited an irreversible oxidation wave because of the instability of resulting R-TCNQ-OMe$^\bullet$ species ($E_p^{ox} = +0.48$ V for R = Me; $-+0.88$ V for R = F_4 vs. SCE in MeCN), revealed that their electron-donating abilities are much stronger than **C** ($E_p^{ox} = +1.90$ V vs. SCE in MeCN)[14] and can act as electron-donors to R-TCNQ. The differences between E_p^{ox} of R-TCNQ-OMe$^-$ salts and $E_{1/2}^{red}$ of corresponding R-TCNQ ($\Delta E^{redox} = E^{ox} - E^{red}$) were in the range from +0.27 to +0.31 V, and these values were smaller than the upper limit of ΔE^{redox} of CT between donor and acceptor, +0.34 V for low-dimensional TTF·TCNQ systems.[16a] Actually, the reaction between salt **1** and neutral F_4TCNQ in MeCN afforded a deep blue solid of salt **2**.[1a] Accordingly, the simplest mechanism to produce R-TCNQ$^{\bullet-}$ in Groups **II** and **III** appeared to proceed through exchange of charge between R-TCNQ-OMe$^-$ and R-TCNQ (Scheme 2, step 2).[19] Thus, in principle, all R-TCNQ derivatives gave salts in Group **I** together with those in Groups **II** and **III**. Since R-TCNQ-OMe$^\bullet$ species might be unstable, these by-products have not been detected.

The reaction of strong R-TCNQ (R = F_4 or CF_3) resulted in very low yield of R-TCNQ$^{\bullet-}$ salts (isolated yield, 3 and 0%, respectively, from the corresponding R-TCNQ, see Supporting Information). In these cases, most of the acceptors were converted to R-TCNQ-OMe$^-$. On the other hand, the reaction of the weaker acceptors (R = F_2, F, H, Me, Et_2, and Me_2) gave a higher yield of R-TCNQ$^{\bullet-}$ salt (isolated yield, 11–30% from corresponding R-TCNQ, see Supporting Information). Although the reason for these results has not been fully determined, we suggest the following possible reasons; very fast reaction between a strong acceptor and MeOH immediately consumes R-TCNQ (Scheme 2, step 1), preventing the succeeding reaction from generating R-TCNQ$^{\bullet-}$ (Scheme 2, step 2). For the reaction of weak acceptors, methanolysis proceeded more slowly, allowing electron transfer from R-TCNQ-OMe$^-$ to surviving R-TCNQ. In the cases of MeTCNQ and Me_2-TCNQ, the larger amount of surviving R-TCNQ would result in the generation of Group **III** salts.

Reaction using other solvents such as water, ethanol (EtOH), 1-propanol, or *t*-butyl alcohol instead of MeOH for **C** also afforded R-TCNQ$^{\bullet-}$ species. However, since reaction using dry DMF as a solvent for **C** also generated TCNQ$^{\bullet-}$, there are other likely processes not involving alcoholysis that yield R-TCNQ$^{\bullet-}$.

Group I: (1) Destructed R-TCNQ Anion Salts. Light-colored compounds in Table 1, **1** (R = F_4),[1a] **3** (R = CF_3), **4** (R = F_2), **6** (R = F), **8** (pristine), and **11** (R = Me) were assigned as ionic salts of destructed R-TCNQ, and all were insulators electrically and silent magnetically. Group **I** solids of Et_2TCNQ and Me_2TCNQ were not isolated. In general, stronger R-TCNQ acceptors gave two kinds of products: ionic salts of Group **I** and 2:1 fully ionic CT salts of Group **II**. It seems that each R-TCNQ provides both destructed R-TCNQ salt of Group **I** and radical anion salt of Group **II** or **III** from one batch, in accordance with the formation mechanism described above. Group **I** salts were soluble in both MeOH and MeCN and obtained from the concentrated solution. In all cases, the isolation of pure products of Group **I**, which should be white to pale yellow (vide infra), was rather difficult and needed careful purification by repeated recrystallization because of decomposition in solution and contamination by R-TCNQ$^{\bullet-}$. The slight green color and very weak absorption bands ascribable to R-TCNQ$^{\bullet-}$ at around 10–20 × 10^3 cm^{-1} in UV–vis spectra of the solids in Group **I** indicated minute contamination by radical anions. In the case of CF_3TCNQ, we have not found appropriate preparation conditions to obtain the Group **II** solid, but the deep green color of the reaction mixture clearly indicates generation of CF_3TCNQ$^{\bullet-}$ species in the reaction.

Figure 1a compares the IR spectra of solid products for pristine TCNQ (**8**–**10**) in the C≡N stretching region. Salt **8** exhibited two characteristic C≡N modes. The first C≡N peaks (2178 cm^{-1}) appeared at a lower frequency by 18 cm^{-1} than that of K$^+$·TCNQ$^{\bullet-}$. Furthermore, the value for the separation of two peaks ($\Delta\nu_{C\equiv N} = 54$ cm^{-1}) was extraordinarily large in comparison with that of K$^+$·TCNQ$^{\bullet-}$ ($\Delta\nu_{C\equiv N} = 14$ cm^{-1}). These results were common for all the compounds of Group **I**, where $\Delta\nu_{C\equiv N}$ = 40–55 cm^{-1}, and first C≡N peak appeared at a lower frequency by 18–21 cm^{-1} than that of R-TCNQ$^{\bullet-}$ salts. These observations unambiguously confirmed that the products in Group **I** did not include R-TCNQ$^{\bullet-}$ molecules.

Figure 1b compares the IR spectra of these products in the C=C and C=O stretching regions. The C=C stretching modes

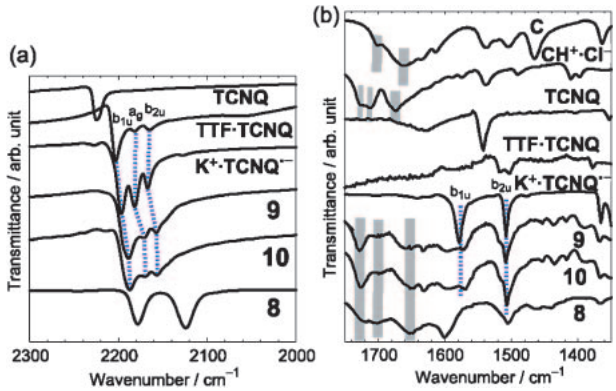

Fig. 1. IR spectra (KBr pellet) of TCNQ salts (**8**–**10**) together with those of related salts and $TTF^{0.59\bullet+}$·$TCNQ^{0.59\bullet-}$ in the (a) C≡N stretching region and (b) C=C and C=O stretching regions. Dotted and thick lines indicate the vibration modes of TCNQ species and **C** species, respectively.

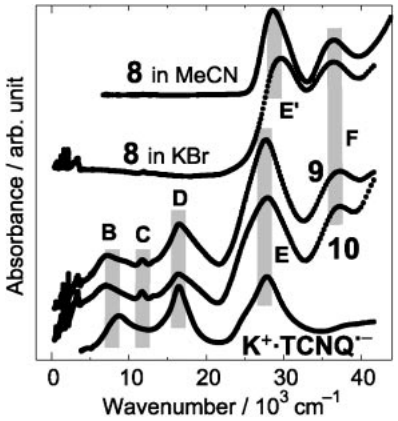

Fig. 2. UV–vis–NIR spectra of TCNQ salts (**8**–**10**) and K^+·$TCNQ^{\bullet-}$. Lines are drawn as a guide for eyes.

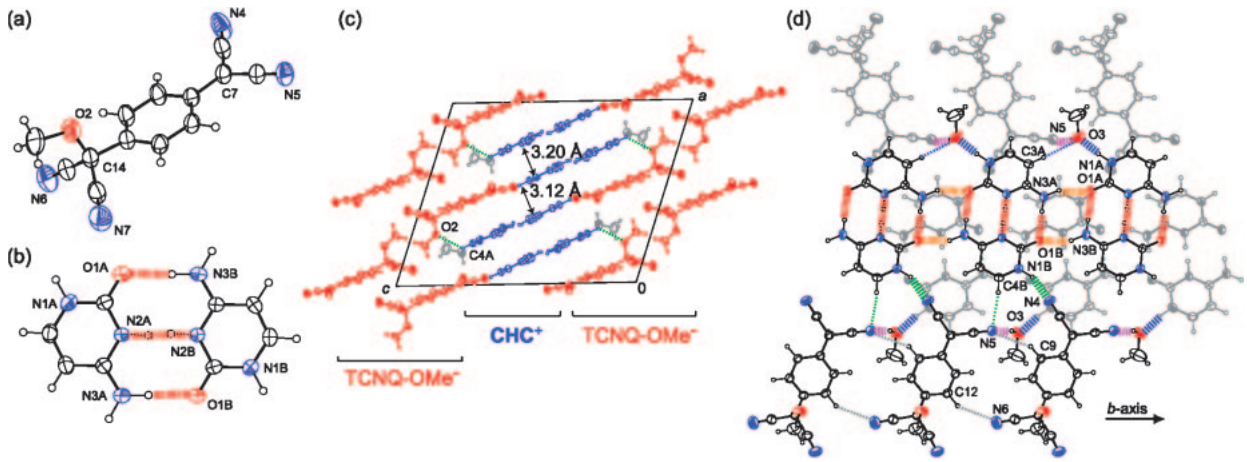

Fig. 3. Molecular and crystal structures of salt **8**. Molecular structures of (a) TCNQ-OMe^- and (b) $\mathbf{CHC}^+$ pair. (c) Layered structures of TCNQ-OMe^- (red) and $\mathbf{CHC}^+$ pair (blue) viewed along the *b*-axis. Gray molecules show MeOH molecules. (d) HB structure including the one-dimensional $\mathbf{CHC}^+$ ribbon structure. Dotted lines indicate HBs.

of **8** did not show good correspondence with those of K^+·$TCNQ^{\bullet-}$, indicating considerable skeletal change of TCNQ. The C=O stretching modes in the 1750–1650 cm^{-1} range provide information concerning **C** species. Strong peaks at 1727, 1710, and 1674 cm^{-1} have been observed in protonated $\mathbf{CH}^+$, while such modes appeared at 1701 and 1662 cm^{-1} for neutral **C**. The spectrum of **8** was not a simple superimposition of those of **C** and $\mathbf{CH}^+$, but is reminiscent of that in the cytidinium–cytidine pair (1725, 1700, and 1665 cm^{-1}).[21] Thus, the **C** moiety of **8** contained the $\mathbf{CHC}^+$ species or its analogs. These features were common for all products in Group **I**.

Figure 2 presents the UV–vis–NIR spectrum of **8** displaying intense bands at 29.8 and 36.5 × 10^3 cm^{-1} (labeled as Bands E′ and F, respectively). These bands did not shift when the medium was changed from KBr to MeCN. Band-F was ascribed to an intramolecular transition of protonated **C** species from comparison with $\mathbf{CH}^+$·Cl^- (35.9 × 10^3 cm^{-1}). Accordingly, Band-E′ was assignable to an intramolecular transition of the anion species. There was no significant absorption below 25 × 10^3 cm^{-1} originating from R-$TCNQ^{\bullet-}$ species. These features were common for all products in Group **I** (Band-E′ at 28.9–30.3 × 10^3 and Band-F at 36.2–37.9 × 10^3 cm^{-1}, see Table 1).

Group I. (2) Crystal Structure of 8. Chemical species of Group **I** products were identified for **1**[1a] and **8** by crystal structure analysis. Single crystals of **8** were obtained by recrystallization from MeOH as yellow platelets including MeOH as a crystal solvent instead of water molecules of the powder sample (Table 2). Figure 3 shows the molecular and crystal structures of **8**, ($\mathbf{CHC}^+$)(TCNQ-OMe^-)(MeOH), and Table 3 summarizes the short intermolecular HB interactions.

The bond length of C14–O2 (1.412(4) Å (1 Å = 0.1 nm)) in TCNQ-OMe^- (Fig. 3a) undoubtedly proves the formation of a σ-bond. TCNQ-OMe^- molecules were arranged as a layer parallel to the *ab* plane (Fig. 3c). **C** molecules formed an asymmetric $\mathbf{CHC}^+$ unit by triple complementary HBs (two N3–H···O1 bonds and one N2A···H···N2B bond, thick red lines in Fig. 3b). It is known that protonation of **C** increases the C–N–C bond angle of N2 by ca. 5° (neutral **C**: 119.3° and $\mathbf{CH}^+$: 124.3°).[23] In the crystal structure of **8**, the C–N–C bond

Table 3. Bond Lengths[a)] of Short HBs between **C**···**C** in a $\mathbf{CHC}^+$ Pair, $\mathbf{CHC}^+$···$\mathbf{CHC}^+$, $\mathbf{CHC}^+$···TCNQ-OMe$^-$, TCNQ-OMe$^-$···TCNQ-OMe$^-$, $\mathbf{CHC}^+$···MeOH, and MeOH···TCNQ-OMe$^-$ Molecules in **8**[b)]

	D–H···A	H···A/Å	D···A/Å
$\mathbf{CHC}^+$	N2A–H···N2B	1.86	2.84
	N2A···H–N2B	1.85	2.84
	N3A–H···O1B	1.85	2.84
	N3B–H···O1A	1.88	2.88
$\mathbf{CHC}^+$···$\mathbf{CHC}^+$	N3A–H···O1A	1.96	2.91
	N3B–H···O1B	1.94	2.88
$\mathbf{CHC}^+$···TCNQ-OMe$^-$	N1B–H···N4≡C5	1.89	2.84
	C4B–H···N5≡C6	2.37	3.31
	C4A–H···O2	2.57	3.27
TCNQ-OMe$^-$···TCNQ-OMe$^-$	C9–H···N5≡C6	2.67	3.59
	C12–H···N6≡C15	2.65	3.57
$\mathbf{CHC}^+$···MeOH	N1A–H···O3	1.76	2.74
	C3A–H···O3	2.63	3.61
MeOH···TCNQ-OMe$^-$	O3–H···N5≡C6	1.87	2.83

a) Å (1 Å = 0.1 nm). b) Sum of van der Waals radii: N···N, 3.10; N···O, 3.07; O···O, 3.04; C···N, 3.25; C···O, 3.22; H···N, 2.75; H···O, 2.72 Å.[22]

angles of two **C** moieties were close to each other (122.1(3)° for N2A and 120.7(3)° for N2B) indicating that the proton of $\mathbf{CHC}^+$ unit disordered between N2A and N2B atoms. Therefore, protons were placed on both N2A and N2B atoms with a site occupancy factor of 0.5. The $\mathbf{CHC}^+$ units were connected by double complementary HBs (N3–H···O1 bonds, thick orange lines in Fig. 3d) giving a linear infinite ribbon along the *b*-axis. The ribbon stacked to form a zigzag motif with interplanar distances of 3.20 and 3.12 Å along the *a*-axis (Fig. 3c). The polycationic layer comprising $\mathbf{CHC}^+$ ribbons and polyanionic layer comprising TCNQ-OMe$^-$ array were arranged alternately along the *c*-axis to construct a layered ionic salt (Fig. 3c). As shown in Figs. 3c and 3d, there were short HBs between $\mathbf{CHC}^+$ and TCNQ-OMe$^-$ (N1B–H···N4≡C, C4B–H···N5≡C, and C4A–H···O2; thick and thin green lines), between $\mathbf{CHC}^+$ and MeOH (N1A–H···O3 and C3A–H···O3, thick and thin blue lines, respectively), between TCNQ-OMe$^-$ and MeOH (O3–H···N5≡C, thick purple lines), and between TCNQ-OMe$^-$ molecules (C9–H···N5≡C and C12–H···N6≡C, thin gray lines) (Table 3).

Group II: Fully Ionic CT Salts. (1) Optical Spectra. Products **2** (R = F_4),[1a] **5** (R = F_2), **7** (R = F), **9**,[1b] **10** (pristine), and **13** (R = Et_2) belonged to Group **II**. IR and UV–vis–NIR spectra of **9** and **10** are depicted in Figs. 1 and 2 as representatives. Figure 1a compares the $\nu_{C\equiv N}$ modes of **9** and **10** with those of $TCNQ^0$, $K^+\cdot TCNQ^{\bullet-}$, and $TTF^{0.59\bullet+}\cdot TCNQ^{0.59\bullet-}$. The neutral TCNQ has a single absorption at 2222 cm^{-1}, and $K^+\cdot TCNQ^{\bullet-}$ has three distinguishable modes at 2196 (b_{1u}), 2182 (a_g), and 2166 (b_{2u}) cm^{-1}.[24a] The strong appearance of a_g mode in $K^+\cdot TCNQ^{\bullet-}$ is ascribed to lattice distortion caused by dimerization. The $\nu_{C\equiv N}$ modes of $TTF^{0.59\bullet+}\cdot TCNQ^{0.59\bullet-}$ having a uniform segregated stack shows a strong b_{1u} mode, weak a_g and b_{2u} modes.[24b]

The $\nu_{C\equiv N}$ modes of **9** and **10** (2187–2188, 2170, and 2157 cm^{-1}) differed from those of the TCNQ-OMe$^-$ species in **8** and resembled each other and $K^+\cdot TCNQ^{\bullet-}$ except for the considerable weakening of a_g and b_{2u} modes and softening of each mode by 8–12 cm^{-1}. The weak appearance of a_g mode in **9** and **10** at 2170 cm^{-1} suggested the formation of a uniform stacking as seen in $TTF^{0.59\bullet+}\cdot TCNQ^{0.59\bullet-}$. It is known that the $\nu_{C\equiv N}$ (b_{1u}) mode of TCNQ CT solids softens linearly with ionicity; sharply up to $\delta \approx 0.5$ and very dully in the range of $\delta = 0.5$–1.[24c] The b_{1u} modes of **9** and **10** showed a greater softening than that of $K^+\cdot TCNQ^{\bullet-}$ and consequently did not give precise information for δ of TCNQ molecules. A similar softening by 1–12 cm^{-1} for the first C≡N mode was seen in other solids in Group **II** (Table 1). This behavior is caused by the environmental perturbations around the C≡N groups probably because of the HB interactions (see crystal structure analyses of **9** and **13**, vide infra). Therefore, only a combination of the IR and UV–vis–NIR spectra could provide clear evidence of the fully ionic state of R-TCNQ for products of Group **II** (**2**, **5**, **7**, **9**, **10**, and **13**) and partial CT or mixed-valent state for products in Group **III** (**12** and **14**) as discussed later.

Contrary to the environmental sensitivity of C≡N stretching modes, the C=C stretching modes of TCNQ are almost insensitive to environmental perturbations.[25] In TCNQ CT solids, C=C stretching modes exhibit large ionization shifts. The C=C modes at 1570 and 1508 cm^{-1} for **9** and 1574 and 1507 cm^{-1} for **10** corresponded excellently to those of $TCNQ^{\bullet-}$ (1578–1580 for b_{1u} and 1504–1508 cm^{-1} for b_{2u})[25b] indicating that the TCNQ moiety in **9** and **10** was fully ionic $TCNQ^{\bullet-}$ (Fig. 1b). The C=C stretching modes of TCNQ moieties of **9** and **10** in the Raman spectra (1403 and 1402 cm^{-1}, respectively, see Supporting Information) also corresponded to that of $TCNQ^{\bullet-}$ (1384 cm^{-1}) rather than that of neutral TCNQ (1454 cm^{-1}).[26] The C=O modes in the IR spectra (1750–1650 cm^{-1}) of **9** and **10** (indicated by thick lines in Fig. 1b) exhibited similar features to those of **8**, three broad peaks at 1726–1727, 1698–1706, and 1651–1653 cm^{-1}, and this observation indicated the presence of a $\mathbf{CHC}^+$ species or its analogs.

The UV–vis–NIR spectra of **9** and **10** (Fig. 2) in KBr pellet exhibited close similarity to that of $K^+\cdot TCNQ^{\bullet-}$ (Bands B–E). Band-B is assigned as an intermolecular transition of $TCNQ^{\bullet-}$ within a segregated column.[27] Band-C is ascribed to either the interdimer transition or intramolecular transition of monomeric $TCNQ^{\bullet-}$.[27] Bands D and E are assigned as intramolecular transitions of $TCNQ^{\bullet-}$.

The spectral features of **9** and **10** as well as all compounds in Group **II** were similar to those of fully ionized R-$TCNQ^{\bullet-}$ salts (see Supporting Information). Accordingly, the 1:1 (**10**) or 2:1 (**2**, **5**, **7**, **9**, and **13**) stoichiometry of the CT solid suggested the formula of ($\mathbf{CH}^+$)(R-$TCNQ^{\bullet-}$) or ($\mathbf{CHC}^+$)(R-$TCNQ^{\bullet-}$), respectively. In addition, the appearance of Band-B in all salts in Group **II** implied the formation of segregated structures.

Group II. (2) Structural Properties of 9.[1b] Single crystals suitable for structural analysis were obtained only for **9**[1b] and **13** in Group **II**. The structural analyses of **9** were performed at 9 and 200 K, and the results were essentially the same (see Supporting Information). Therefore, the following discussions are based on the results obtained at 200 K.

In the crystal structure of **9**, one **C** and half of the TCNQ molecules were crystallographically independent. The bond lengths and angles of TCNQ molecules are relevant to the monoanion of TCNQ,[28] and δ on TCNQ was estimated as

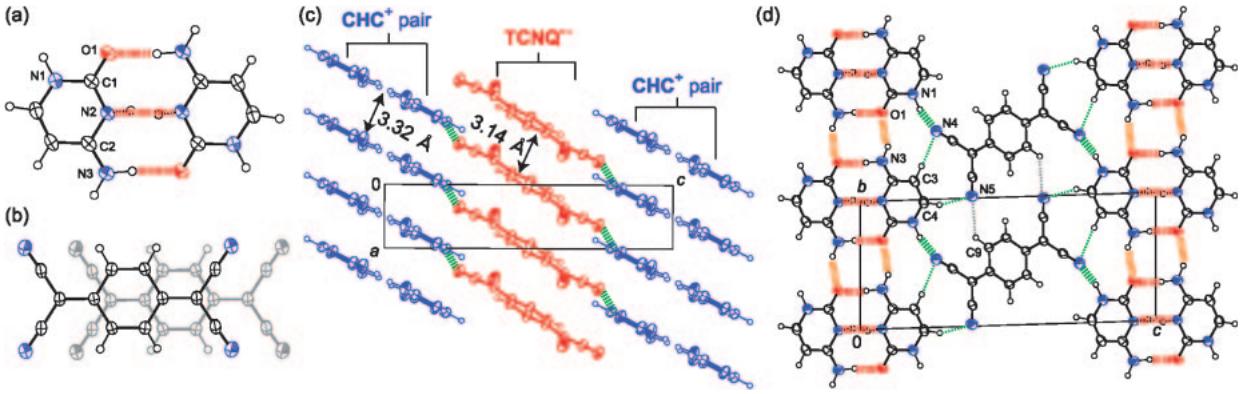

Fig. 4. Molecular and crystal structures of salt **9**.[1b] (a) Molecular structure of **CHC**$^+$ pair. (b) Overlap mode of TCNQ molecules in the one-dimensional column. (c) Layered structures of TCNQ$^{\bullet-}$ (red) and **CHC**$^+$ pair (blue) viewed along the *b*-axis. (d) HB sheet structure including one-dimensional ribbon structures of **CHC**$^+$ viewed along the *a*-axis. Dotted lines indicate HBs.

1.01 to 1.04 based on bond length analysis.[29] **C** molecules formed a symmetric **CHC**$^+$ pair by triple complementary HBs (two N3–H···O1 and one N2–H···N2 bonds, dotted red lines in Fig. 4a). Since the inversion center was located at the center of a pair, the hydrogen atom on N2 disordered in two sites with a site occupancy factor of 0.5. The C–N–C bond angle of N2 was 121.6(3)° and close to the average of those of neutral **C** (119.3°) and protonated **CH**$^+$ (124.3°)[23] in good agreement with the half-protonation of **C** moiety in this salt.

Individual TCNQ molecules formed a segregated stack along the *a*-axis (Fig. 4c). The TCNQ column possessed a bond-over-ring overlap fashion (Fig. 4b) with an interplanar distance (*d*) of 3.14 Å, which was considerably short, even though the thermal effect is taken into account, compared to the fully ionic TCNQ salts having uniform segregated columns ($d \geq 3.248$ Å at RT) observed so far.[28] Within the experimental accuracy of X-ray structural analysis, dimerization was not detected in the TCNQ column down to 9 K ($d = 3.10$ Å). TCNQ molecules were arranged to form a narrow TCNQ ribbon (8.23 Å wide) along the *b*-axis with the aid of weak HBs between TCNQ molecules (C9–H···N5≡C, thin gray lines in Fig. 4d). The overlap integral along the stacking direction ($S = 20.4 \times 10^{-3}$) exceeded those of other directions ($S < 10^{-4}$) indicating a one-dimensional electronic character.

The **CHC**$^+$ unit also formed a segregated column along the *a*-axis with an interplanar distance of 3.32 Å, where the centers of the **CHC**$^+$ units were collinear (Fig. 4c). The **CHC**$^+$ units were connected with neighboring units by double complementary HBs (N3–H···O1, thick orange lines) along the *b*-axis to form a linear infinite ribbon with a narrow width of 9.10 Å (Fig. 4d). The HB distances in the ribbon suggested the robust nature of the architecture (Table 4).

Two kinds of ribbons of **CHC**$^+$ and TCNQ were linked together by strong (N1–H···N4≡C, thick green lines) and weak (C3–H···N4≡C and C4–H···N5≡C, thin green lines) HBs, and the HB network formed a two-dimensional thin sheet composed of **CHC**$^+$ ribbons and TCNQ ribbons (Fig. 4d). Then, the thin sheets generated a succession of parallel sheets along the *a*-axis to construct the three-dimensional crystal packing. Along the *c*-axis, the alternate stacking of **CHC**$^+$ and TCNQ$^{\bullet-}$ layers formed a layered architecture (Fig. 4d).

Low-dimensional electronic structures of organic metals and Mott insulators are known to be very susceptible to lattice distortions (Peierls or spin-Peierls instability), which originate from strong electron–phonon coupling or spin–phonon coupling.[30a,31] Therefore, conventional Mott type M$^+$•TCNQ$^{\bullet-}$ salts (M = alkali metal) easily dimerize above 200 K.[28,30a] However, the uniform interplanar distance in the TCNQ column of **9** was preserved down to 9 K. The suppression of the lattice distortions along the stacking axis for a wide temperature range can be explained by the following consideration.

Table 4. Bond Lengths[a)] of Short HBs between **C**···**C** in a **CHC**$^+$ Pair, **CHC**$^+$···**CHC**$^+$, **CHC**$^+$···TCNQ, and TCNQ···TCNQ Molecules in **9**[b)]

	D–H···A	H···A/Å	D···A/Å
CHC$^+$	N2–H···N2	1.94	2.84
	N3–H···O1	1.86	2.84
CHC$^+$···**CHC**$^+$	N3–H···O1	2.02	2.88
CHC$^+$···TCNQ	N1–H···N4≡C5	1.94	2.88
	C4–H···N5≡C6	2.37	3.33
	C3–H···N4≡C5	2.74	3.73
TCNQ···TCNQ	C9–H···N5≡C6	2.58	3.36

a) Å (1 Å = 0.1 nm). b) Sum of van der Waals radii: N···N, 3.10; N···O, 3.07; C···N, 3.25; H···N, 2.75; H···O, 2.72 Å.[22]

Group II. (3) Mechanism of Stabilization of TCNQ Columns. The stabilization energies of a **CHC**$^+$ pair were evaluated as −45 and −16 kcal mol^{-1} for the side-by-side (HB interaction) and face-to-face directions (π–π interaction), respectively, using theoretical calculation at the MP2/6-31G level.[32] Notably, the experimental dimerization energy of TCNQ$^{\bullet-}$ estimated in solution (−10.4 kcal mol^{-1})[33] is much smaller than the interaction energies between **CHC**$^+$ units. Because of the robustness of HBs between two kinds of ribbons in **9**, the monomer–dimer transition of TCNQ$^{\bullet-}$ molecules along the stacking direction required a large lattice energy to generate coherent and simultaneous dimerization of the whole two-dimensional sheets (Fig. 4d). Therefore, these intermolecular interactions; the strong self-assembling nature of **CHC**$^+$ to form a one-dimensional ribbon in the side-by-side direction and the robust HBs between **C** and TCNQ molecules, cooperatively prevented the lattice distortion. The structural features of **9** strongly suggested that the robust and uniform HB net-

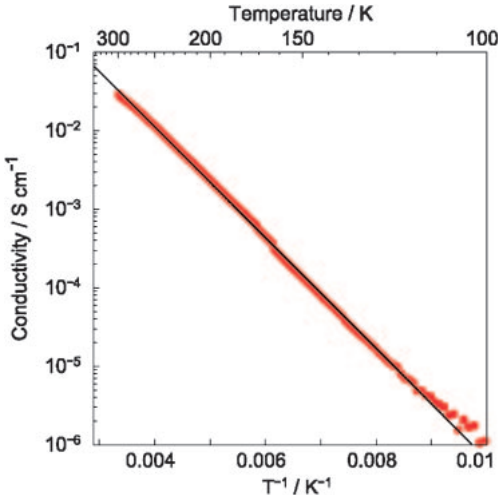

Fig. 5. Arrhenius plot of electrical conductivity of **9** (//*a*).[1b]

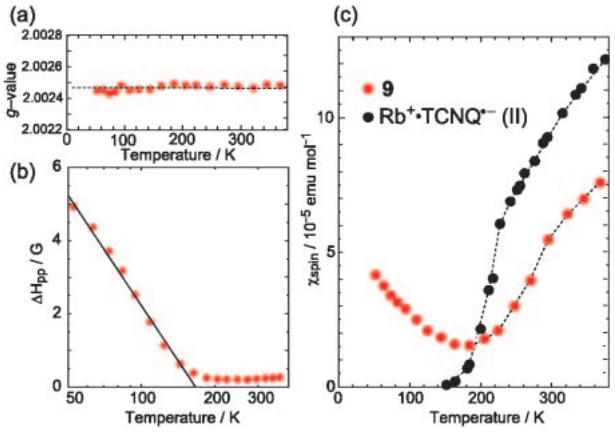

Fig. 6. EPR parameters of **9**. Temperature dependence of (a) *g*-value, (b) ΔH_{pp}, and (c) χ_{spin} (H_0 // *a*, red circles) above 50 K along with that of Rb^+•$TCNQ^{•-}$(II) (black circles).[38]

work would strengthen the system against lattice distortions even when the system has a low-dimensional electronic structure. This result would provide a prototype for the study of the relationship between HBs and transport properties and suggest a new strategy of suppressing the Peierls instability necessary to help in the development of superconductors.[31a]

Group II. (4) Conductivity and Magnetic Properties. Conductivity data of the salts in Group **II** are summarized in Table 2. The conductivity measurements for a single crystal of **9** and compressed pellets of others showed that **2** was a good insulator ($\sigma_{RT} = 5.3$–6.4×10^{-9} S cm^{-1}), and the other salts in Group **II** were rather good semiconductors with σ_{RT} of 3×10^{-2} to 4×10^{-5} S cm^{-1}.

Figure 5 shows an Arrhenius plot of electrical conductivity of a single crystal of **9**. The σ_{RT} of **9** was 2.7–3.2×10^{-2} S cm^{-1} with ε_a of 0.14 eV (//*a*). It should be emphasized that the σ_{RT} value of **9** was higher than any other fully ionized TCNQ salts known so far.[28d,30] The high conductivity as a fully ionic salt was ascribed to the large overlap integral in a TCNQ column caused by a short interplanar distance ($d =$ 3.14 Å at 200 K) with a bond-over-ring type overlap and uniform stacking manner.

The EPR parameters of **9** (*g*-value, linewidth (ΔH_{pp}), and spin susceptibility (χ_{spin})) for a single crystal along the conduction direction of TCNQ columns (H_0 // *a*) are summarized in Fig. 6. A single Lorentzian signal was observed down to 50 K, below which the EPR spectra of each crystal differed owing to the effect of defect spin. Therefore, we will discuss EPR data above 50 K. The angle dependence of *g*-values indicated that the signal was solely ascribed to $TCNQ^{•-}$ ($g =$ 2.0025–2.0030 (//*ab*) and 2.0024–2.0028 (//*ac*), which agreed with the reported *g*-values for $TCNQ^{•-}$ ($g_{min} = 2.0020$ and $g_{max} = 2.0032$)[34]). The constant *g*-value against temperature indicated that there was no orientation change of $TCNQ^{•-}$ (Fig. 6a). Fine structure which has been detected in the dimeric form of M^+•$TCNQ^{•-}$[35] was not observed. Above 180 K, the signal was very sharp ($\Delta H_{pp} =$ ca. 0.2 G, Fig. 6b), and the χ_{spin} increased with temperature (Fig. 6c, red circles). The χ_{spin} value at 296 K (5.5×10^{-5} emu mol^{-1}) corresponded to 4.4% of the non-interacting total spins for $S = 1/2$ ($\chi_{spin} = 1.25 \times 10^{-3}$ emu mol^{-1} at 300 K), indicating that almost all spins were magnetically inactive owing to the strong antiferromagnetic exchange in a uniform chain ($J/k_B =$ ca. -700 K in $T > 240$ K).[36] The magnitude of χ_{spin} and its temperature dependence were similar to those of M^+•$TCNQ^{•-}$ salts in the Mott insulating phase (i.e. $\chi_{spin} = 0.8$–2.4×10^{-4} emu mol^{-1} at 420 K for M = K, Cs, Rb^{II}, and NH_4).[37,38] For example, the χ_{spin} of Rb^+•$TCNQ^{•-}$ (II) decreases almost linearly with temperature ($\chi_{spin} = 0.9$–1.0×10^{-4} at 300 K) and then extinguishes by dimerization at 220 K, which is a characteristic behavior of the spin-Peierls transition (Fig. 6c, black circles).[38] On the other hand, **9** did not exhibit any spin-gap formation above 180 K. Furthermore, the constant and sharp linewidth down to 180 K also denied the antiferromagnetic ordering in **9** above 180 K.

Below 180 K, both χ_{spin} and ΔH_{pp} increased with decreasing temperature (Figs. 6b and 6c). A plot of ΔH_{pp} vs. $\ln T$ (Fig. 6b) indicated a similar linear relation that was observed in quinolinium(TCNQ)$_2$ below 20 K, in which ΔH_{pp} was interpreted within a random-exchange Heisenberg antiferromagnetic chain (REHAC) model with a spin of $S = 1/2$.[39]

In the temperature dependence of static susceptibility (χ_{stat}) of polycrystals of **9**, χ_{stat} increased with the temperature above 180 K (see Supporting Information), similar to that observed for χ_{spin}. Below 150 K, χ_{stat} of defect spin followed the Curie law with $C = 1.34 \times 10^{-3}$ emu K mol^{-1} which corresponded to 0.36% of independent $S = 1/2$ spins. After subtracting the Curie paramagnetism, the RT value of χ_{stat} was 4.5×10^{-5} emu mol^{-1} corresponding to 3.6% of spin. The analysis based on the singlet–triplet model[36] above 240 K resulted in the $J/k_B =$ ca. -700 K of antiferromagnetic interaction in **9**.

Although **9** did not structurally and magnetically exhibit significant phase transition such as spin-Peierls transition, the temperature dependence of reflectance spectra (polarization //*a*-axis) showed that the a_g vibration modes, which are very sensitive to lattice distortion, grew with decreasing temperature down to 200 K (see Supporting Information). This behavior corresponds to the growth of antiferromagnetic coupling within the uniform TCNQ column and is seen in the M^+•$TCNQ^{•-}$ spin-Peierls systems.[24a,30d] In salt **9**, spin pairing would cause slight and random dimerization in the TCNQ col-

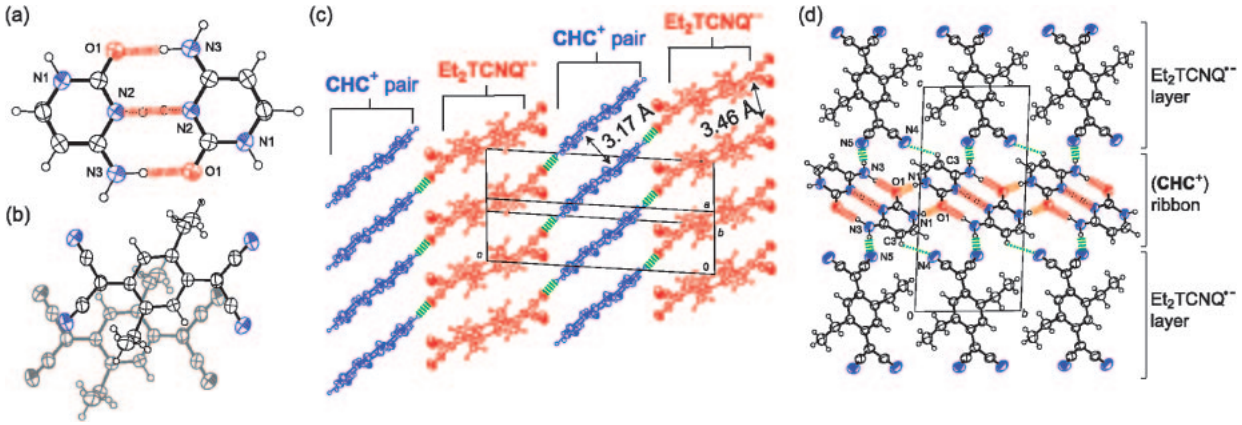

Fig. 7. Molecular and crystal structures of salt **13**. (a) Molecular structure of $\mathbf{CHC}^+$ pair. (b) Overlap mode of Et_2TCNQ molecules in the one-dimensional column. (c) Layered structures of $Et_2TCNQ^{\bullet-}$ (red) and $\mathbf{CHC}^+$ pair (blue). (d) HB sheet structure including the one-dimensional ribbon structure of $\mathbf{CHC}^+$ viewed along the *a*-axis. Dotted lines indicate HBs.

umn; however, the robust and uniform HB network prevented the distinguishable three-dimensional ordering as discussed above.

The magnetic behavior of **9** in the whole temperature region is very similar to that of 1,6-diaminopyrene (DAP)·TCNQ complex which is a nearly fully ionic complex (δ = ca. 0.9) containing a small amount of neutral components as defect (spin-0 soliton) and forms uniform segregated columns preserved down to low temperature (118 K).[40] The χ_{spin} (ca. 8×10^{-5} emu mol^{-1} at RT) of this complex gradually decreases down to ca. 100 K without abrupt spin quenching and then increases due to the Curie impurity.[40b]

Summarizing the magnetic properties of **9**, the strong antiferromagnetic interaction in a uniform $TCNQ^{\bullet-}$ column quenched the spins resulting in only a few active spins at RT, and the spin pairing proceeded with decreasing temperature down to 180 K. However, abrupt spin ordering such as spin-Peierls transition was not observed. This behavior is consistent with the absence of lattice dimerization in structural analyses and contrasts with other conventional one-dimensional $TCNQ^{\bullet-}$ systems. For the other **C**–R-$TCNQ^{\bullet-}$ salts in Group **II** (**5**, **7**, **10**, and **13**), the absence of abrupt phase transition in electrical conductivity and magnetic measurement even at low temperature indicated that they did not exhibit significant monomer–dimer phase transitions (see Supporting Information). These results suggest that these salts are resistant to lattice distortion due to the formation of robust HB network structures as seen in salt **9**.

Group II. (5) Crystal Structure of 13. Figure 7 shows the molecular and crystal structures of **13**, and Table 5 summarizes the short HB lengths in this crystal. In the crystal structure, one **C** and a half of Et_2TCNQ molecules were crystallographically independent. This salt showed similar structural features to those of **9**, a one-dimensional ribbon of $\mathbf{CHC}^+$ pairs linked by the complementary HBs, uniform Et_2TCNQ column, and alternate stacking of $\mathbf{CHC}^+$ and Et_2TCNQ layers. Only the HB pattern in a $\mathbf{CHC}^+$ ribbon and the overlap mode in an Et_2TCNQ column were different from those of **9**.

The triple complementary HBs formed a $\mathbf{CHC}^+$ pair (two N3–H···O1 and one N2–H···N2 bonds, dotted red lines in Fig. 7a). Similar to **9**, the $\mathbf{CHC}^+$ pair possessed an inversion center at its center, and the hydrogen atom on N2 disordered into two sites with site occupancy of 0.5. The C–N–C bond angle of N2 (121.1(4)°) also agreed with the half-protonation of **C** moiety. $\mathbf{CHC}^+$ units formed a one-dimensional ribbon structure in a zigzag pattern in terms of the double complementary HBs between the imino nitrogen (N1) on the pyrimidine-ring and the carbonyl oxygen (O1) (Fig. 7d, orange lines). The $\mathbf{CHC}^+$ ribbons stacked along the *a*-axis with an interplanar distance of 3.17 Å to form a polycationic layer (Fig. 7c).

Table 5. Bond Lengths[a)] of Short HBs between **C**···**C** in a $\mathbf{CHC}^+$ Pair, $\mathbf{CHC}^+$···$\mathbf{CHC}^+$, and $\mathbf{CHC}^+$···Et_2TCNQ Molecules in **13**[b)]

	D–H···A	H···A/Å	D···A/Å
$\mathbf{CHC}^+$	N2–H···N2	1.80	2.80
	N3–H···O1	1.82	2.82
$\mathbf{CHC}^+$···$\mathbf{CHC}^+$	N1–H···O1	1.84	2.83
$\mathbf{CHC}^+$···Et_2TCNQ	N3–H···N5≡C6	1.91	2.91
	C3–H···N4≡C5	2.72	3.38

a) Å (1 Å = 0.1 nm). b) Sum of van der Waals radii: N···N, 3.10; N···O, 3.07; C···N, 3.25; H···N, 2.75; H···O, 2.72 Å.[22]

Et_2TCNQ molecules stacked uniformly to form a one-dimensional column along the *a*-axis (Fig. 7c). Because of a small overlapping pattern (Fig. 7b) and large interplanar distance (3.46 Å), the overlap integral along the stacking direction ($S = 7.4 \times 10^{-3}$) was smaller than that of salt **9**. The Et_2TCNQ columns were arranged along the *b*-axis to form a layered structure (Fig. 7d). The $\mathbf{CHC}^+$ and Et_2TCNQ layers stacked alternately along the *c*-axis to construct the three-dimensional structure of this crystal. Short N3–H···N5≡C and C3–H···N4≡C HBs were observed between $\mathbf{CHC}^+$ and Et_2TCNQ layers, and these HBs formed a two-dimensional sheet structure (Fig. 7d, thick and thin green lines).

Group III. Partially Ionic or Mixed-Valent CT Salts. MeTCNQ and Me_2TCNQ afforded products in this class, **12** and **14**, respectively. The first C≡N stretching mode of **12** appeared at 2202 cm^{-1} between those of neutral MeTCNQ (2223 cm^{-1}) and $MeTCNQ^{\bullet-}$ (2190 cm^{-1}) (Fig. 8a). Although the C≡N stretching mode did not give correct information about the ionicity of the acceptor, the softening in **12** by

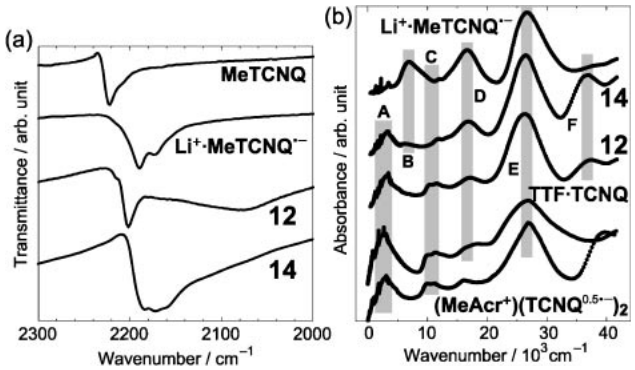

Fig. 8. (a) IR spectra (C≡N region) and (b) UV–vis–NIR spectra of salts **12** and **14** together with those of the related salts (KBr pellet). Assignment of Bands A–F is mentioned in the text. $MeAcr^+$: *N*-methylacridinium.

$21\,cm^{-1}$ from neutral MeTCNQ indicated its highly ionized state. The C=O stretching modes of **C** moiety in **12** (see Supporting Information) resembled those of **8** and **9**, which contained the $\mathbf{CHC}^+$ cation, and indicated the existence of $\mathbf{CHC}^+$ or analogous species. The UV–vis–NIR spectrum of **12** clearly showed a Band-A below $5 \times 10^3\,cm^{-1}$ and no Band-B at around 7–8 $\times 10^3\,cm^{-1}$, confirming a partially ionic (uniform charge) or mixed-valent (non-uniform charge) nature ($\delta \leq 0.5$) in **12** (Fig. 8b).[16,27,30a] In particular, the spectrum of **12** was very similar to those of metallic complex $TTF^{0.59\bullet+}$·$TCNQ^{0.59\bullet-}$ and highly conductive complex $(MeAcr^+)(TCNQ^{0.5\bullet-})_2$ ($MeAcr^+$ = *N*-methylacridinium, σ_{RT} = ca. $100\,S\,cm^{-1}$ on single crystal and $2\,S\,cm^{-1}$ on pellet sample)[41] even in the splitting of Band-C. In the Raman spectrum, **12** exhibited a single C=C stretching mode (ν_4) at $1420\,cm^{-1}$, indicating the uniform charge of MeTCNQ (see Supporting Information). Accordingly, the optical data and elemental analysis presented a formula, $(\mathbf{CHC}^+)(MeTCNQ^{0.5\bullet-})_2$ for **12**.

This salt was the most conductive one in this study (σ_{RT} = 2.7–7.2 $\times 10^{+1}\,S\,cm^{-1}$, single crystal samples obtained from EtOH–benzonitrile (PhCN), see Fig. S1f in Supporting Information) and exhibited a metallic behavior down to $T_{\sigma max}$ of 273–289 K (Fig. 9a). Below $T_{\sigma max}$, the resistivity gradually increased with decreasing temperature, and no abrupt jump was observed. However, the thin shape and poor quality of single crystals even prepared under the best condition so far examined prevented us from confirming the metallic nature at lower temperatures based on transport and optical analyses. The static magnetic susceptibility measurements showed an almost temperature independent χ_{stat} suggesting Pauli-like paramagnetism down to low temperatures (Fig. 9b; $\chi_{RT} = 4.7 \times 10^{-4}$, $\chi_{40\,K} = 3.6 \times 10^{-4}\,emu\,mol^{-1}$).

Me_2TCNQ salt **14** also exhibited Band-A at around $3.4 \times 10^3\,cm^{-1}$, indicating the partially ionized or mixed-valent state of Me_2TCNQ (Fig. 8b). In addition, a weak Band-B was observed at $6.2 \times 10^3\,cm^{-1}$, which implied the existence of a dimerized $(Me_2TCNQ^{\bullet-})_2$ unit or larger ionicity than 0.5. The first C≡N stretching mode of **14** ($\nu_{CN} = 2184\,cm^{-1}$), which is close to that of monoanion ($2183\,cm^{-1}$), also confirmed the highly ionized state (Fig. 8a). The Raman spectrum of **14** showed two ν_4 modes at 1444 and $1408\,cm^{-1}$. Assuming a linear relation between δ of Me_2TCNQ and ν_4 (Me_2TCNQ^0: $1452\,cm^{-1}$ and $Me_2TCNQ^{\bullet-}$: $1392\,cm^{-1}$),[42] δ values in **14** were estimated as 0.13 and 0.73. This feature is similar to that of $(Me_4As^+)_2(Me_2TCNQ)_3$ salt (ν_4 = 1441–1442 and 1407–$1409\,cm^{-1}$).[42] From these spectral properties and elemental analysis, **14** is deduced as a mixed-valent salt (non uniform charge) with an averaged δ of 2/3, $(\mathbf{C_3H}^+)_2(Me_2TCNQ^{\delta'\bullet-})_2$-$(Me_2TCNQ^{\delta''\bullet-})(H_2O)$, where the $\mathbf{C_3H}^+$ is an unknown species, and $2\delta' + \delta'' = 2$. The electrical conductivity measurement revealed the semiconducting nature of salt **14** (σ_{RT} = 2.6–4.7 $\times 10^{-2}\,S\,cm^{-1}$, ε_a = 0.081–0.085 eV, compaction pellets); however, the conductivity was lower than that of **12** by a magnitude of three orders. The χ_{stat} value at RT ($7.0 \times 10^{-5}\,emu\,mol^{-1}$) in the magnetic susceptibility measurement revealed the strong antiferromagnetic interaction of $Me_2TCNQ^{\bullet-}$ molecules which agreed with the appearance of Band-B in UV–vis–NIR spectrum and lower conductivity than **12**.

Structural Regulation in $\mathbf{CHC}^+$ Salts. The ability to form intermolecular HBs is important in the construction of biomolecule architecture or for supramolecular chemistry and crystal engineering.[2–6] Although its definitive roles for electron transport have not been clarified yet, some researchers have suggested several key methodologies to assist electron

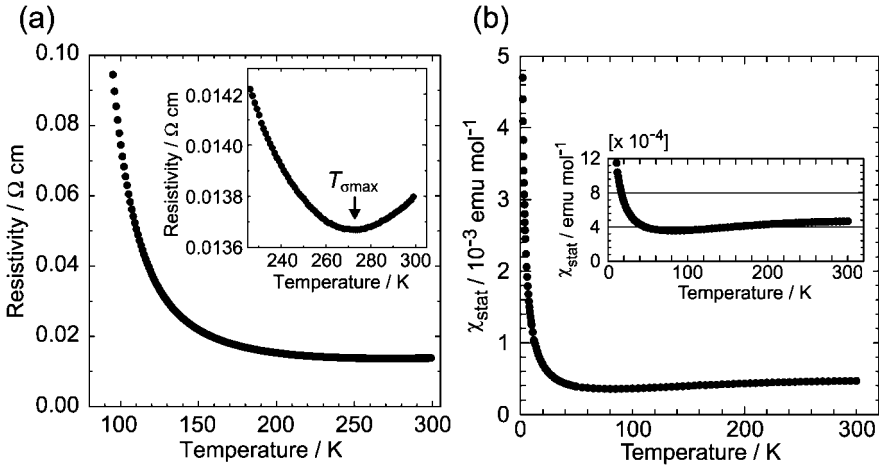

Fig. 9. (a) Temperature dependence of resistivity of salt **12** down to 100 K measured for the single crystal (inset shows the expansion around RT). (b) Temperature dependence of χ_{stat} for a polycrystalline sample (inset shows the expansion) of salt **12**.

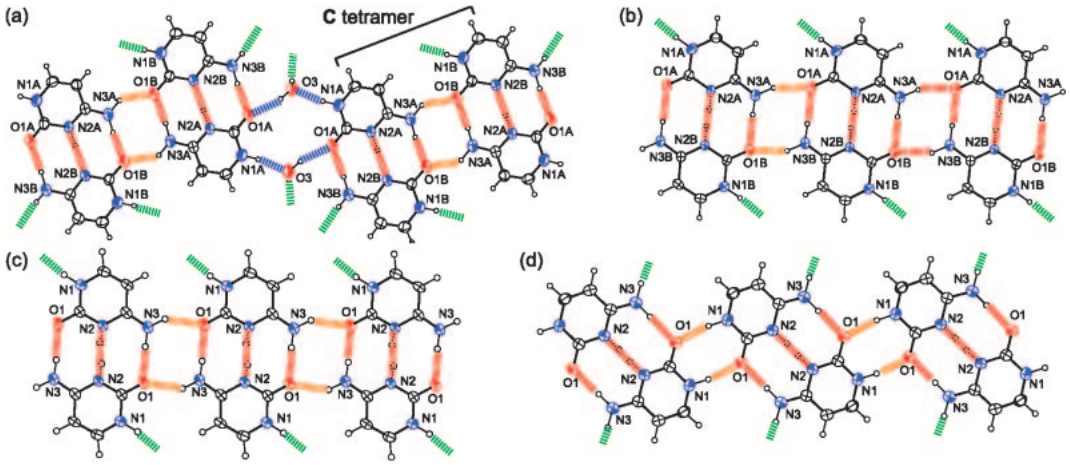

Fig. 10. HB patterns in one-dimensional **CHC**$^+$ ribbons of **1**,[1a] **8**, **9**,[1b] and **13** (a–d, respectively). HBs are illustrated by dotted lines for **CHC**$^+$ units (red), direct **CHC**$^+$···**CHC**$^+$ units (orange), water mediated **CHC**$^+$···**CHC**$^+$ units (blue), and **CHC**$^+$ with other molecules (green).

transport using HB interactions; (1) control of molecular arrangement,[43] (2) increase of the electronic dimensionality of network structures, (3) control of component ratio in CT solid based on the molecular recognition forming donor–acceptor pairs,[44] and (4) modification of redox ability of electron donors and acceptors based on high polarizability.[44b,45] Moreover, we have reported that (5) HB in the CT solid decreases conduction gap[46a] and (6) the HB should produce a uniform transfer integral (t) rather than an alternating one.[46b] Non-uniform and alternating HBs give rise to a dimerized band structure generated by two kinds of t and a narrow HOMO band, which is highly susceptible to the electron correlation U_{eff}.

Figure 10 illustrates the HB patterns in one-dimensional ribbons of **CHC**$^+$ units constructed in salts **1**,[1a] **8**, **9**,[1b] and **13**, where six HBs involving N1, N2, N3, and O1 atoms were formed to stabilize their structures. The HB patterns in **8** and **9** possessed linear shape and were very similar to each other with differences only in their symmetry (Figs. 10b and 10c). Neighboring **CHC**$^+$ units were linked parallel to each other by double HBs between the amino nitrogen (N3) and the carbonyl oxygen (O1) atoms (orange lines). This type of HB ribbons has been observed in $[Ni(nta)(H_2O)_2](\mathbf{CHC}^+)\cdot 2H_2O$ (nta: nitrilotriacetate),[18i] where the ribbons stacked to form a layered structure as seen in salts **8** and **9**. In the case of salt **13**, the double HBs between the imino nitrogen (N1) on the pyrimidine-ring and the carbonyl oxygen (O1) atoms connected **CHC**$^+$ units to form a zigzag ribbon motif in **13** (Fig. 10d, orange lines). This type of ribbon structure has been reported in two salts, $(\mathbf{CHC}^+)_2[ZnCl_4]$[18c] and $(\mathbf{CHC}^+)[BF_4]$.[18k] These salts included an asymmetric **CHC**$^+$, which was different from the symmetric one in **13**. In both cases, the π-stacking of **CHC**$^+$ ribbons produced layered structures. The water molecules in the **CHC**$^+$ ribbon of salt **1** increased the variation of the HB pattern (Fig. 10a). The double N3A–H···O1B HBs (orange lines), which were observed in salts **8** and **9**, formed a **C** tetramer (dimer of **CHC**$^+$). The tetramer was linked by double HBs between N1 and O1 atoms through water molecules (N1A–H···O3–H···O1A, blue lines), which were similar to the linkage in **CHC**$^+$ in **13** and formed a zigzag ribbon.

The HB interaction of **CHC**$^+$ played a critical role in the construction of a segregated structure, which is one of the necessary conditions to construct highly conductive CT solids. In the crystal structures of **1**,[1a] **8**, **9**,[1b] and **13**, the π-stacking of **CHC**$^+$ ribbons formed polycationic layers. The HB formation of **CHC**$^+$ ribbons with R-TCNQ$^{\bullet-}$ or R-TCNQ-OMe$^-$ (green lines in Fig. 10) aligned the anion molecules along the stacking direction of **CHC**$^+$ units to form the anion columns and layered structures of R-TCNQ$^{\bullet-}$ or R-TCNQ-OMe$^-$ (in the case of **8**, the TCNQ-OMe$^-$ layer did not involve a π-stacking column, Fig. 3c). Furthermore, the uniform arrangement of **CHC**$^+$ units along both HB ribbon and stacking directions should be one of the key factors in the formation and strengthening of the uniform columnar structures of salts **9** and **13**. Although the crystal structures have not been elucidated in the salts **5**, **7**, **10**, and **12**, the HB interactions would play important roles in the construction of the uniform segregated structures as evidenced by the optical, conductivity, and magnetic measurements.

Conclusion

We have investigated the reaction of **C** and R-TCNQ derivatives in MeOH solution. The reaction yielded dark blue-black solids of R-TCNQ$^{\bullet-}$ salts in spite of the poor electron-donating ability of **C** and produced pale-colored solid products of the destructed TCNQ anion, R-TCNQ-OMe$^-$. For the TTF·TCNQ system, the ionization of component molecules occurs in the redox range of $\Delta E^{\mathrm{redox}} < +0.34$ V.[16a] Amazingly, the weakest acceptor in Table 1, Me_2TCNQ and Et_2TCNQ ($E^{\mathrm{red}} = +0.15$ V vs. SCE), which cannot be ionized by BEDT-TTF ($E_{1/2}{}^{\mathrm{ox}} = +0.53$ V vs. SCE, $\Delta E^{\mathrm{redox}} = +0.38$ V), afforded radical salts **13** and **14**, respectively, with **C** ($\Delta E^{\mathrm{redox}} = +1.75$ V).[14] The radical cations of **C** were not obtained, and the cation units in solid products were clarified as protonated **C** species ($\mathbf{C}_n\mathbf{H}^+$, n = 1–3), where the hemiprotonated pair ($n = 2$, **CHC**$^+$) was the most common. The products were classified into three groups based on the electronic structure of the anion species: (**I**) insulating σ-bonded R-TCNQ-OMe$^-$ salts, (**II**) fully ionized R-TCNQ$^{\bullet-}$ salts, and (**III**) highly conductive partially ionized or mixed-valent R-TCNQ$^{\delta\bullet-}$ salts ($0 < \delta < 1$). From the analysis of these reac-

tion products, a tentative reaction mechanism was proposed, (1) methanolysis of R-TCNQ, (2) deprotonation by **C**, and (3) one-electron transfer from R-TCNQ-OMe$^-$ to neutral R-TCNQ.

The structural analyses of salts **1**[1a] and **8** in Group **I** and salts **9**[1b] and **13** in Group **II** showed that **C** molecules in these salts formed the hemiprotonated **CHC**$^+$ pair by triple complementary HBs. The double complementary HBs between **CHC**$^+$ pairs established the one-dimensional ribbon structures which stacked by π–π interaction to construct two-dimensional layers. Furthermore, the ability of **CHC**$^+$ ribbon to form strong HBs with R-TCNQ$^{\bullet-}$ or R-TCNQ-OMe$^-$ established the segregated layered structures, one of the most essential criteria for conducting CT solids. This structural regulation ability of the **CHC**$^+$ system demonstrated two intriguing systems: (1) the most conductive salt as a fully ionic TCNQ salt (**9**, $\sigma_{RT} = 3 \times 10^{-2}$ S cm^{-1}) exhibiting a robust uniform stacking structure and no three-dimensional structural ordering even at low temperature and (2) the most conductive CT salt showing metallic behavior (**12**, $\sigma_{RT} = 2.7$–$7.2 \times 10^{+1}$ S cm^{-1}, $T_{\sigma max} = 273$–289 K) as a CT complex based on biological materials.

Biomolecule-based conductors with robust and highly ordered self-assembled structures have attracted many materials scientists. The investigation of CT complexes of **C** in the present work will provide a new strategy for the development of conducting electronic materials based on biological systems. One of the further interests of biological molecule based conductors is the hole-transport phenomena of DNA wire, where the one-dimensional π-stack of nucleobases is presumed to form the conduction path.[47] Although **C** could not cause conduction in the present study due to protonation during complex formation, the investigation of CT solids of nucleobases will be able to provide vital information of the electrical conduction of DNA molecules.

Experimental

General. **C** (98%) was used as purchased since CT solids prepared using purified **C** did not show any significant difference in the kinds of products and their physical properties. R-TCNQs except for pristine TCNQ were synthesized in our laboratory and were purified by crystallization and/or sublimation.

Conductivity Measurements. DC conductivities of the CT solids were measured by a standard four- or two-probe technique using gold wires of 10–50 μm diameter using gold paste (Tokuriki, 8560-1A).

Optical Measurements. Measurements of absorption spectra were done with a KBr disk on a Perkin-Elmer PARAGON 1000 Series FT-IR (resolution 2 or 4 cm^{-1}) for IR and near-IR regions (400–7800 cm^{-1}), and on a SHIMADZU UV-3100 spectrometer for near-IR, visible, and ultraviolet (UV–vis–NIR) regions (3800–42000 cm^{-1}). Raman spectra were collected using a Renishaw Ramascope System 1000 composed of a notch filter, single monochromator and charge-coupled device cooled by a thermoelectric device. Excitation light from a He-Ne laser, NEC GLG5731 (632.8 nm) was focused on a ca. 10 μm diameter spot through a microscope equipped with an objective lens Mitsutoyo M Plan Apo 20×. The scatter light was collected with a backscattering geometry.

Magnetic Measurements. EPR spectra were measured by a JEOL JES-RE2X X Band EPR spectrometer equipped with temperature controller Oxford EPR-900 cryostat in a temperature range of 1.9–350 K. The DC magnetic susceptibility was measured at a field of 0.5 or 1.0 T with an MPMS-XL Quantum Design SQUID magnetometer in a temperature range of 2–300 K in an atmosphere of helium.

X-ray Crystallography. The intensity data of the structural analysis were collected using an oscillator type X-ray imaging plate (DIP-2020K) with monochromated Mo Kα radiation. The structures were solved by direct method using SHELXS-97.[48] Refinements of structure were achieved by full-matrix least-squares method (SHELXL-97).[49] Positions of hydrogen atoms were determined by assuming the sp^2 or sp^3 configuration of each atom with an X–H (X = C, N, and O) distance of 1.0 Å for others. Parameters were refined by adopting anisotropic and isotropic temperature factors for non-hydrogen and hydrogen atoms, respectively. Selected crystallographic data were summarized in Supporting Information. Crystallographic data have been deposited with Cambridge Crystallographic Data Centre: Deposition numbers CCDC 612487 (**1**), 667897 (**8**), 602000 (**9**, 200 K), 602001 (**9**, 9 K), and 664138 (**13**). Copies of the data can be obtained free of charge via http://www.ccdc.cam.ac.uk/conts/retrieving.html (or from the Cambridge Crystallographic Data Centre, 12, Union Road, Cambridge, CB2 1EZ, UK; Fax: +44 1223 336033; e-mail: deposit@ccdc.cam.ac.uk).

Cyclic Voltammetry Measurements. Cyclic voltammetric measurement was carried out in a solution of 0.1 M Bu_4NBF_4 in MeCN vs. SCE by means of an ALS/chi Electrochemical Analyzer Model 650 A at room temperature. The experiments employed a Pt plate working electrode, a Pt wire counter electrode, and a SCE reference electrode.

Band Structure Calculation. Band structure was calculated based on the crystal structure by the extended Hückel tight-binding method with single ζ parameters.

Typical Procedure for the Reaction between Cytosine and R-TCNQ: Preparation of 4 and 5. Cytosine (112 mg, 1.01 mmol) was dissolved in MeOH (40 mL). To this mixture, a solution of F_2TCNQ (240 mg, 1.00 mmol) in MeCN (40 mL) was added. The reaction mixture was left to stand at −18 °C for 3 days. The resulting solid was collected by filtration, and then washed with MeOH (1 mL × 3), to give salt **5** (80.2 mg, 17% from F_2TCNQ) as deep blue needle crystals. The filtrate was concentrated, and the residue was suspended in MeOH (5 mL). The insoluble precipitate was removed by filtration. The filtrate was concentrated, and the residue was washed with MeCN (1 mL) and ether (3 mL). The resulting powder was dissolved in MeOH (5 mL) and then treated with charcoal (10 mg). After concentration, the residue was recrystallized from MeOH (1 mL)–ethyl acetate (10 mL) at −18 °C, to give salt **4** (30.4 mg, 5% from F_2TCNQ) as a pale green powder. The high solubility of salt **4** caused the low isolated yield.

This work was partly supported by a Grant-in-Aid (21st Century COE programs on Kyoto University Alliance for Chemistry and No. 15205019) from the Ministry of Education, Culture, Sports, Science and Technology, Japan. T.M. is a recipient of a Japan Society for the Promotion of Science (JSPS) research fellowship.

Supporting Information

Selected physical data, UV–vis–NIR and IR spectra of all products, temperature dependence of reflectance spectra of **9**, Raman

spectra (**9**, **10**, **12**, and **14**), temperature dependence of magnetic susceptibility and electrical conductivity for products in Groups **II** and **III**, pictures of crystalline products (**1**, **8**, **9**, **12**, and **13**), crystallographic data of **1**, **8**, **9** (9 and 200 K), and **13**, and cyclic voltammetry of products in Group **I**. This material is available free of charge at http://www.csj.jp/journals/bcsj/.

References

1 Preliminary accounts of part of this work: a) The products of F_4TCNQ (**1** and **2**), see: T. Murata, G. Saito, *Chem. Lett.* **2006**, *35*, 1342. b) The radical anion salt of TCNQ (**9**), see: T. Murata, K. Nishimura, G. Saito, *Mol. Cryst. Liq. Cryst.* **2007**, *466*, 101.

2 a) J.-M. Lehn, *Supramolecular Chemistry*, VCH, Weinheim, **1995**. b) N. C. Seeman, *Nature* **2003**, *421*, 427. c) E. Katz, I. Willner, *Angew. Chem., Int. Ed.* **2004**, *43*, 6042.

3 a) R. Foster, *Organic Charge-Transfer Complexes*, Academic Press, New York, **1969**, Chap. 12. b) J. B. Birks, M. A. Slifkin, *Nature* **1963**, *197*, 42. c) E. M. Kosower, *Molecular Biochemistry*, McGraw-Hill, New York, **1962**. d) Y. Matsunaga, *Nature* **1966**, *211*, 182. e) U. Thewalt, C. E. Bugg, *Acta Crystallogr., Sect. B* **1972**, *28*, 82. f) M. Tanaka, *Bull. Chem. Soc. Jpn.* **1977**, *50*, 3194. g) G. Saito, A. K. Colter, *Tetrahedron Lett.* **1977**, *18*, 3325. h) M. Suzuki, T. Fujii, T. Nogami, T. Hirano, T. Ishida, *Chem. Lett.* **2006**, *35*, 250.

4 a) G. A. Jeffrey, *An Introduction to Hydrogen Bonding*, Oxford University Press, New York, **1997**. b) G. A. Jeffrey, W. Saenger, *Hydrogen Bonding in Biological Structures*, Springer, Berlin, **1991**. c) G. R. Desiraju, T. Steiner, *The Weak Hydrogen Bond*, Oxford University Press, New York, **1999**.

5 a) J. D. Watson, F. H. C. Crick, *Nature* **1953**, *171*, 737. b) W. Saenger, *Principles of Nucleic Acid Structure*, 1st ed., Springer-Verlag, New York, **1984**.

6 a) *Chem. Mater.* **1994**, *6*, No. 8. b) *Organic Molecular Solids, Properties and Applications*, ed. by W. Jones, CRC Press, New York, **1997**, Chap. 6. c) J. L. Sessler, C. M. Lawrence, J. Jayawickramarajah, *Chem. Soc. Rev.* **2007**, *36*, 314.

7 a) Y. Morita, S. Maki, M. Ohmoto, H. Kitagawa, T. Okubo, T. Mitani, K. Nakasuji, *Org. Lett.* **2002**, *4*, 2185. b) M. Ohmoto, S. Maki, Y. Morita, T. Kubo, H. Kitagawa, T. Okubo, T. Mitani, K. Nakasuji, *Synth. Met.* **2003**, *133–134*, 337. c) E. Miyazaki, Y. Morita, Y. Umemoto, K. Fukui, K. Nakasuji, *Chem. Lett.* **2005**, *34*, 1326. d) Y. Morita, E. Miyazaki, Y. Umemoto, K. Fukui, K. Nakasuji, *J. Org. Chem.* **2006**, *71*, 5631. TTF derivative having adenine moiety, see: e) Y. Morita, S. Maki, M. Ohmoto, H. Kitagawa, T. Okubo, T. Mitani, K. Nakasuji, *Synth. Met.* **2003**, *135–136*, 541. TTF derivative having cytosine moiety, see: f) E. Miyazaki, Y. Morita, Y. Yakiyama, S. Maki, Y. Umemoto, M. Ohmoto, K. Nakasuji, *Chem. Lett.* **2007**, *36*, 1102.

8 a) O. Neilands, V. Tilika, I. Sudmale, I. Grigorjeva, A. Edzina, E. Fonavs, I. Muzikante, *Adv. Mater. Opt. Electron.* **1997**, *7*, 39. b) O. Neilands, *Mol. Cryst. Liq. Cryst.* **2001**, *355*, 331. c) K. Balodis, S. Khasanov, C. Chong, M. Maesato, H. Yamochi, G. Saito, O. Neilands, *Synth. Met.* **2003**, *133–134*, 353.

9 M. A. Slifkin, A. P. Kushelevsky, *Spectrochim. Acta, Part A* **1971**, *27*, 1999.

10 I. N. Bazhina, V. S. Verzilov, V. S. Grechishkin, R. V. Grechishkina, V. M. Gusarov, *Zh. Strukt. Khim.* **1973**, *14*, 930.

11 G. G. Sheina, E. D. Radchenko, Y. P. Blagoi, B. I. Verkin, *Dokl. Akad. Nauk SSSR* **1978**, *240*, 463.

12 a) V. M. Orlov, A. N. Smirnov, Y. M. Varshavsky, *Tetrahedron Lett.* **1976**, *17*, 4377. b) D. Dougherty, E. S. Younathan, R. Voll, S. Abdulnur, S. P. McGlynn, *J. Electron Spectrosc. Relat. Phenom.* **1978**, *13*, 379. c) S. G. Lias, J. E. Bartmess, J. F. Liebman, J. L. Holmes, R. D. Levin, W. G. Mallard, *J. Phys. Chem. Ref. Data* **1988**, *17*, 861. d) S. D. Wetmore, R. J. Boyd, L. A. Eriksson, *Chem. Phys. Lett.* **2000**, *322*, 129, and references are therein.

13 a) A. J. Berlinsky, J. F. Carolan, L. Weiler, *Can. J. Chem.* **1974**, *52*, 3373. b) N. Sato, G. Saito, H. Inokuchi, *Chem. Phys.* **1983**, *76*, 79.

14 C. A. M. Seidel, A. Schulz, M. H. M. Sauer, *J. Phys. Chem.* **1996**, *100*, 5541.

15 a) W. Flossmann, E. Westhof, A. Müller, *Int. J. Radiat. Biol.* **1976**, *30*, 301. b) J. Geimer, K. Hildenbrand, S. Naumov, D. Beckert, *Phys. Chem. Chem. Phys.* **2000**, *2*, 4199.

16 a) G. Saito, J. P. Ferraris, *Bull. Chem. Soc. Jpn.* **1980**, *53*, 2141. b) S. Horiuchi, H. Yamochi, G. Saito, K. Sakaguchi, M. Kusunoki, *J. Am. Chem. Soc.* **1996**, *118*, 8604. c) T. Senga, K. Kamoshida, L. A. Kushch, G. Saito, T. Inayoshi, I. Ono, *Mol. Cryst. Liq. Cryst.* **1997**, *296*, 97. d) S.-S. Pac, G. Saito, *J. Solid State Chem.* **2002**, *168*, 486.

17 *Data for Biochemical Research*, 3rd ed., ed. by R. M. C. Dawson, W. H. Elliot, K. M. Jones, Clarendon Press, Oxford, **1986**.

18 a) R. E. Marsh, R. Bierstedt, E. L. Eichhorn, *Acta Crystallogr.* **1962**, *15*, 310. b) T. J. Kistemacher, M. Rossi, L. G. Marzilli, *Biopolymers* **1978**, *17*, 2581. c) F. Fujinami, K. Ogawa, Y. Arakawa, S. Shirotake, S. Fujii, K. Tomita, *Acta Crystallogr., Sect. B* **1979**, *35*, 968. d) E. Westhof, M. Sundaralingam, *Proc. Natl. Acad. Sci. U.S.A.* **1980**, *77*, 1852. e) M. Gdaniec, B. Brycki, M. Szafran, *J. Chem. Soc., Perkin Trans. 2* **1988**, 1775. f) K. Gehring, J.-L. Leroy, M. Guéron, *Nature* **1993**, *363*, 561. g) L. Chen, L. Cai, X. Zhang, A. Rich, *Biochemistry* **1994**, *33*, 13540. h) S. Metzger, B. Lippert, *Angew. Chem., Int. Ed. Engl.* **1996**, *35*, 1228. i) Md. A. Salam, K. Aoki, *Inorg. Chim. Acta* **2000**, *311*, 15. j) J. Müller, E. Freisinger, *Acta Crystallogr., Sect. E* **2005**, *61*, o320. k) D. Armentano, G. De Munno, R. Rossi, *New J. Chem.* **2006**, *30*, 13.

19 K. Tanemura, Y. Nishida, T. Suzuki, K. Satsumabayashi, T. Horaguchi, *J. Chem. Res., Synop.* **1999**, 40.

20 The generation of TCNQ-OMe^- (C≡N modes: 2187 and 2124 cm^{-1}) in the reaction between $[Mn^{3+}(saltmen^{2-})(H_2O)]$-$ClO_4^-$ (saltmen^{2-}: *N*,*N*′-(1,1,2,2-tetramethylethylene)bis(salicylideneiminato)) and $Li^+ \cdot TCNQ^{\bullet -}$ in MeOH has been reported, see: H. Miyasaka, K. Sugimoto, K. Sugiura, T. Ishii, M. Yamashita, *Mol. Cryst. Liq. Cryst.* **2002**, *379*, 197.

21 B. Borah, J. L. Wood, *J. Mol. Struct.* **1976**, *30*, 13.

22 A. Bondi, *J. Phys. Chem.* **1964**, *68*, 441.

23 N. S. Mandel, *Acta Crystallogr., Sect. B* **1977**, *33*, 1079.

24 a) H. Okamoto, Y. Tokura, T. Koda, *Phys. Rev. B* **1987**, *36*, 3858. b) S. Etemad, *Phys. Rev. B* **1981**, *24*, 4959. c) J. S. Chappell, A. N. Bloch, W. A. Bryden, M. Maxfield, T. O. Poehler, D. O. Cowan, *J. Am. Chem. Soc.* **1981**, *103*, 2442. It should be noted that the authors of this paper used both b_{1u} and a_g modes of C≡N stretching in their analysis. If one uses only b_{1u} modes of IR spectra, the linear relation between $\nu_{C\equiv N}$ and the degree of CT (δ) is held only below $\delta = 0.5$.

25 a) M. Meneghetti, C. Pecile, *J. Chem. Phys.* **1986**, *84*, 4149. b) C. J. Fritchie, P. Arthur, *Acta Crystallogr.* **1966**, *21*, 139. c) K. D. Cummings, D. B. Tanner, J. S. Miller, *Phys. Rev. B* **1981**, *24*, 4142.

26 S. Matsuzaki, R. Kuwata, K. Toyoda, *Solid State Commun.* **1980**, *33*, 403.

27 a) J. B. Torrance, B. A. Scott, B. Welber, F. B. Kaufman, P. E. Seiden, *Phys. Rev. B* **1979**, *19*, 730. b) J. B. Torrance, *Acc. Chem. Res.* **1979**, *12*, 79. c) S. Yamaguchi, Y. Moritomo, Y. Tokura, *Phys. Rev. B* **1993**, *48*, 6654. d) M. Meneghetti, *Phys. Rev. B* **1994**, *50*, 16899.

28 a) M. Konno, Y. Saito, *Acta Crystallogr., Sect. B* **1974**, *30*, 1294. b) M. Konno, Y. Saito, *Acta Crystallogr., Sect. B* **1975**, *31*, 2007. c) M. Konno, T. Ishii, Y. Saito, *Acta Crystallogr., Sect. B* **1977**, *33*, 763. d) H. Kobayashi, *Bull. Chem. Soc. Jpn.* **1981**, *54*, 3669. e) H. Kobayashi, *Acta Crystallogr., Sect. B* **1978**, *34*, 2818.

29 a) P. S. Flandrois, D. Chasseau, *Acta Crystallogr., Sect. B* **1977**, *33*, 2744. b) T. J. Kistenmacher, T. J. Emge, A. N. Bloch, D. O. Cowan, *Acta Crystallogr., Sect. B* **1982**, *38*, 1193.

30 a) *Semiconductors and Semimetals: Highly Conducting Quasi-One-Dimensional Organic Crystals*, ed. by E. M. Conwell, Academic Press, New York, **1988**, Vol. 27. b) L. R. Melby, R. J. Harder, W. R. Hertler, W. Mahler, R. E. Benson, W. E. Mochel, *J. Am. Chem. Soc.* **1962**, *84*, 3374. c) N. Sakai, I. Shirotani, S. Minomura, *Bull. Chem. Soc. Jpn.* **1972**, *45*, 3314. d) R. Bozio, C. Pecile, *J. Chem. Phys.* **1977**, *67*, 3864.

31 a) T. Ishiguro, K. Yamaji, G. Saito, *Organic Superconductors*, 2nd ed., Springer-Verlag, Berlin, **1998**. b) D. Jérome, H. J. Schulz, *Adv. Phys.* **1982**, *31*, 299.

32 J. Šponer, J. Leszczynski, V. Vetterl, P. Hobza, *J. Biomol. Struct. Dyn.* **1996**, *13*, 695.

33 R. H. Boyd, W. D. Phillips, *J. Chem. Phys.* **1965**, *43*, 2927.

34 C. Coulon, R. Clérac, *Chem. Rev.* **2004**, *104*, 5655.

35 T. Hibma, J. Kommandeur, *Phys. Rev. B* **1975**, *12*, 2608.

36 The χ_{spin} and χ_{stat} values ($T > 240$ K) were fitted by the singlet–triplet model, see: B. Bleaney, K. D. Bowers, *Proc. R. Soc. London, Ser. A* **1952**, *214*, 451.

37 J. Kommandeur, in *The Physics and Chemistry of Low Dimensional Solids*, ed. by L. Alcácer, D. Reidel Pub., Dordrecht, **1980**, pp. 197–212.

38 J. G. Vegter, J. Kommandeur, *Mol. Cryst. Liq. Cryst.* **1975**, *30*, 11.

39 L. C. Tippie, W. G. Clark, *Phys. Rev. B* **1981**, *23*, 5854.

40 a) T. Inabe, K. Okaniwa, H. Ogata, H. Okamoto, T. Mitani, Y. Maruyama, *Acta Chim. Hung.* **1993**, *130*, 537. b) T. Sekikawa, H. Okamoto, T. Mitani, T. Inabe, Y. Maruyama, T. Kobayashi, *Phys. Rev. B* **1997**, *55*, 4182.

41 K. Holczer, A. Jánossy, *Solid State Commun.* **1978**, *26*, 689.

42 C. Nakano, K. Yakushi, M. Kohama, K. Ueda, T. Sugimoto, *Solid State Commun.* **2000**, *113*, 677.

43 M. Fourmiguè, P. Batail, *Chem. Rev.* **2004**, *104*, 5379, and references therein.

44 a) T. Murata, Y. Morita, K. Fukui, K. Sato, D. Shiomi, T. Takui, M. Maesato, H. Yamochi, G. Saito, K. Nakasuji, *Angew. Chem., Int. Ed.* **2004**, *43*, 6343. b) T. Murata, Y. Morita, Y. Yakiyama, K. Fukui, H. Yamochi, G. Saito, K. Nakasuji, *J. Am. Chem. Soc.* **2007**, *129*, 10837.

45 a) L. M. Goldenberg, O. Neilands, *J. Electroanal. Chem.* **1999**, *463*, 212. b) A. S. F. Boyd, G. Cooke, F. M. A. Duclairoir, V. M. Rotello, *Tetrahedron Lett.* **2003**, *44*, 303. c) Y. Morita, E. Miyazaki, K. Fukui, S. Maki, K. Nakasuji, *Bull. Chem. Soc. Jpn.* **2005**, *78*, 2014.

46 a) Y. Matsunaga, G. Saito, *Bull. Chem. Soc. Jpn.* **1971**, *44*, 958. b) T. Inoue, H. Yamochi, G. Saito, K. Matsumoto, *Synth. Met.* **1995**, *70*, 1139.

47 For reviews, see: a) B. Giese, *Acc. Chem. Res.* **2000**, *33*, 631. b) M. Taniguchi, T. Kawai, *Physica E* **2006**, *33*, 1, and references therein. For examples of individual works, see: c) J. Ladik, *Acta Phys. Acad. Sci. Hung.* **1960**, *11*, 239. d) M. E. Burnel, D. O. Eley, V. Subramanyan, *Ann. N.Y. Acad. Sci.* **1969**, *158*, 191. e) H.-W. Fink, C. Schönenberger, *Nature* **1999**, *398*, 407. f) D. Porath, A. Bezryadin, S. Vries, C. Dekker, *Nature* **2000**, *403*, 635. g) P. J. De Pablo, F. Moreno-Herrero, J. Colchero, J. Gómez-Herrero, P. Herrero, A. M. Baró, P. Ordejón, J. M. Soler, E. Artacho, *Phys. Rev. Lett.* **2000**, *85*, 4992. h) P. Tran, B. Alavi, G. Gruner, *Phys. Rev. Lett.* **2000**, *85*, 1564. i) A. Y. Kasumov, M. Kociak, S. Guéron, B. Reulet, V. T. Volkov, D. V. Klinov, H. Bouchiat, *Science* **2001**, *291*, 280. j) A. Rakitin, P. Aich, C. Papadopoulos, Y. Kobzar, A. S. Vedeneev, J. S. Lee, J. M. Xu, *Phys. Rev. Lett.* **2001**, *86*, 3670. k) K.-H. Yoo, D. H. Ha, J.-O. Lee, J. W. Park, J. Kim, J. J. Kim, H.-Y. Lee, T. Kawai, H. Y. Choi, *Phys. Rev. Lett.* **2001**, *87*, 198102. l) Y. Zhang, R. H. Austin, J. Kraeft, E. C. Cox, N. P. Ong, *Phys. Rev. Lett.* **2002**, *89*, 198102. m) B. Hartzell, B. McCord, D. Asare, H. Chen, J. J. Heremans, V. Soghomonian, *Appl. Phys. Lett.* **2003**, *82*, 4800. n) M. Taniguchi, H.-Y. Lee, H. Tanaka, T. Kawai, *Jpn. J. Appl. Phys.* **2003**, *42*, L215.

48 G. M. Sheldrick, *Program for the Solution of Crystal Structures*, University of Göttingen, Göttingen, Germany, **1997**.

49 G. M. Sheldrick, *Program for the Refinement of Crystal Structures*, University of Göttingen, Göttingen, Germany, **1997**.